*Article*

# Gas-Sensing Performance of Gadolinium Ferrates with Rod and Butterfly Morphologies

Jianbo Lin [1,2], Ningning Liu [1], Tongxiao Zhang [3], Hongjian Liang [1], Guozheng Zhang [1] and Xiaofeng Wang [1,*]

1   Key Laboratory of Materials Modification by Laser Ion and Electron Beams, Ministry of Education, School of Physics, Dalian University of Technology, Dalian 116024, China
2   Key Laboratory of Fire & Rescue Technology and Equipment, MEM, Shanghai 200032, China
3   Leicester International Institute, Dalian University of Technology, Panjin Campus, Panjin 124221, China; 17355892242@163.com
*   Correspondence: wangxf@dlut.edu.cn

**Abstract:** There is an urgent need to develop a low-cost and high-performance gas sensor for industrial production and daily life. Perovskite-type oxides are appropriate materials for resistive gas sensors. In this paper, two gas-sensing materials of gadolinium orthoferrite ($GdFeO_3$) with rod and butterfly morphologies were obtained by annealing the corresponding precursors at 800 °C in a muffle furnace for 3 h. The precursors of $GdFe(CN)_6 \cdot 4H_2O$ with novel morphologies were prepared by a co-precipitation method at room temperature. The materials were evaluated in terms of their structure, morphology, and gas-sensing performance. The gas sensor based on $GdFeO_3$ rods showed a better sensing performance than the sensor based on $GdFeO_3$ butterflies. It exhibited the largest response value of 58.113 to 100 ppm n-propanol at a relatively low operating temperature of 140 °C, and the detection limit was 1 ppm. The results show that the $GdFeO_3$ rods-based sensor performed well in detecting low concentration n-propanol. The satisfactory gas-sensing performance of the $GdFeO_3$ rods-based sensor may be due to the porous structure and the large percentages of defect oxygen and adsorbed oxygen (37.5% and 14.6%) on the surface. This study broadens the application of $GdFeO_3$ in the gas sensor area.

**Keywords:** gas sensing; $GdFeO_3$; co-precipitation method; n-propanol

## 1. Introduction

With the development of industry, the type and quantity of raw materials are increasing day by day, generating toxic, harmful, and volatile substances in production. At the same time, new materials used in people's daily lives will bring similar problems [1]. Some of the released gases have a risk of explosion when the concentration exceeds a certain amount, while some gases seriously endanger human health, causing a series of diseases, such as allergy, respiratory tract infection, organ canceration, etc. In addition, there is a demand for fast, sensitive, and reliable gas sensing for the fermentation process in the food industry, the detection of aroma quality in cosmetics production, the detection of dangerous goods by customs departments, and the diagnosis of patients' breathing gas by medical departments [2,3]. Driven by the huge demand, many researchers are focusing on gas-sensing devices. Compared with infrared spectroscopy, chemiluminescence analysis, and ultraviolet absorption analysis, resistive gas sensors have the advantages of low cost, simple manufacture, and portability [3]. Among the gas-sensing materials for the resistive gas sensor, metal oxide semiconductors have great advantages, such as easy availability of raw materials, low cost, good stability, etc.

The properties of materials depend not only on the chemical composition, but also on their microstructure. Perovskite oxides, $ABO_3$ (A = rare earth metal, B = transition metal, O = oxygen), have flexible design of composition and doping in A-/B- sites, which makes these materials popular in the fields of physics and chemistry [4]. If the A and B elements are

different, the electrical properties and gas-sensing properties are very different. A variety of compositions have been used in the gas-sensing field. For example, LaFeO$_3$, as a widely studied ABO$_3$ material in the field of gas sensors, has excellent gas sensitivity to ethanol, n-propanol, n-butanol, CO, and formaldehyde gases [5–10]. Sheng et al. synthesized NdFeO$_3$ nano-coral particles by a solvothermal method and a calcination treatment, and the prepared NdFeO$_3$-based sensor showed good gas-sensing performance to ethanol [11]. Huang et al. synthesized SmFeO$_3$ material with a hollow porous microsphere structure by a sol–gel method, and the sensor based on this material showed excellent gas-sensing performance for NO$_2$ gas [12].

In particular, as an excellent luminescent and magnetic material [13,14], GdFeO$_3$ has also been used in lithium-ion batteries [15], photocatalysis [13], and electrocatalysis [16]. However, there are only a few studies focused on GdFeO$_3$-based sensors. Wang et al. synthesized Ca-doped GdFeO$_3$ nanocrystalline by the sol–gel method to detect methanol gas [17]. Lee et al. investigated the gas-sensing performance of Co-doped GdFeO$_3$ and the results demonstrated a stable response to NO$_2$ gas [18]. Another work prepared a NO gas sensor based on porous GdFeO$_3$ [19]. More research and exploration are needed to develop GdFeO$_3$-based gas sensors with high performance.

Perovskite oxides are usually prepared by mechanical methods and treated at ultra-high temperatures. The obtained materials always exist agglomerations of large crystal particles without sufficient porosity for gas-sensing reactions [19]. For a gas-sensing material, larger specific surface area could expose more active sites for reacting with gas molecules. To decrease the agglomeration and enhance the porosity of perovskite oxide materials, various chemical methods are introduced, among which the sol–gel method is the most popular due to its low cost, chemical homogeneity, and ease of obtaining nanocrystals. However, the synthetic process always needs more than 10 h [20]. Inspired by the idea of metal–organic frameworks (MOFs), the use of them in preparing metal oxides are escalating [21–25], this work focuses on a method for preparing perovskite-type metal oxide semiconductors using a mild chemical co-precipitation method, which is environmentally friendly and has high product yield.

In this work, in order to obtain a good GdFeO$_3$-based gas sensor, GdFeO$_3$ rods and butterflies were synthesized via a convenient and eco-friendly co-precipitation method and annealing process. The alcohol–water ratio of the solution, the amount of PVP, and the standing time were changed to regulate and control the morphology of GdFe(CN)$_6$·4H$_2$O precursor and the resultant GdFeO$_3$. Scanning electron microscopy (SEM), X-ray diffraction (XRD), and X-ray photoelectron spectroscopy (XPS) were used to characterize the structures, morphologies, and surface states of the obtained materials. The gas-sensing tests evaluated the performances of the two materials. The results showed that the GdFeO$_3$ rods-based sensor exhibited higher response and better selectivity. Therefore, this morphologically controllable porous GdFeO$_3$ can be a candidate with great potential for detecting n-propanol.

## 2. Experiment

### 2.1. Synthesis of Precursors

In this paper, the precursors were synthesized by a co-precipitation method. There were two different suitable synthesis conditions, the former obtained the butterflylike GdFe(CN)$_6$·4H$_2$O precursor, the latter obtained the rodlike GdFe(CN)$_6$·4H$_2$O precursor. The preparation of the butterflylike GdFe(CN)$_6$·4H$_2$O precursor: 90.2 mg Gd(NO$_3$)$_3$·6H$_2$O, 12 mL absolute ethanol, and 3 mL deionized water were mixed and stirred to form a homogeneous solution. Then, 500 mg polyvinyl pyrrolidone (PVP) was added to the solution and stirring was maintained to ensure that PVP was completely dissolved in the solution. Solution A was obtained. Next, 65.8 mg K$_3$[Fe(CN)$_6$] and 15 mL deionized water were mixed to form transparent and homogeneous solution B with a green-yellow color. Finally, solution B was added to solution A drop by drop while stirring. Then, the mixed solution was left to stand for 12 h. (b) The preparation of the rodlike GdFe(CN)$_6$·4H$_2$O:

90.2 mg $Gd(NO_3)_3 \cdot 6H_2O$, 5 mL absolute ethanol, and 2.5 mL deionized water were mixed and stirred to form homogeneous solution A. Next, 65.8 mg $K_3[Fe(CN)_6]$ and 7.5 mL of deionized water were mixed and stirred to form solution B. Finally, solution B was added to solution A drop by drop and left to stand for 36 h.

### 2.2. Synthesis of GdFeO₃

After centrifugation, the dried precursor was slightly ground into powder and then annealed in muffle furnace at 800 °C for 3 h with a heating rate of 2 °C/min. $GdFeO_3$ rods and $GdFeO_3$ butterflies were obtained.

### 2.3. Characterization of GdFe(CN)₆·4H₂O and GdFeO₃

Scanning electron microscopy (SEM) images were recorded on a FEI Nova NanoSEM 450 field emission scanning electron microscope. X-ray diffraction (XRD) patterns of as-prepared samples were collected by Cu K$\alpha$ radiation ($\lambda$ = 1.5406 Å, Shimadzu Corporation, Kyoto, Japan) with a scanning speed of 5 °/min. X-ray photoelectron spectroscopy (XPS) data were obtained by ESCALAB™ 250Xi equipment with an Al K$\alpha$ X-ray radiation source for excitation.

### 2.4. Fabrication and Measurement of Gas-Sensing Devices

The obtained $GdFeO_3$ powder was mixed with deionized water and ground into paste, then the paste was coated onto a ceramic tube with a small brush. After drying in an oven at 60 °C for 8 h, the four Pt wires connected to the Au electrodes were welded to the base, and then the Ni/Cr alloy heating wire was passed through the hollow ceramic tube and welded to the base to make the heater-type gas-sensing device. After aging at 200 °C for 2 h, the device was ready for gas-sensing tests. The gas-sensing tests were performed on a CGS-8 system (Beijing Elite Technology Co., Ltd., Beijing, China) as shown in Scheme 1. The response of the sensor is generally defined as $R_g/R_a$, where $R_g$ and $R_a$ represent the sensor resistance in the target gas and air, respectively.



testing chamber

gas sensor

CGS-8 Intelligent Gas Sensitivity Analysis System
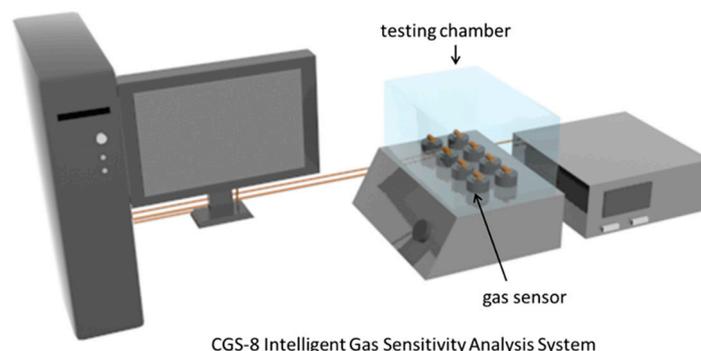
**Scheme 1.** Schematic illustration of the analysis system.

The gases to be measured were obtained from the volatile organic compounds (VOCs), which were liquids at room temperature. Their concentration was calculated according to the following equation:

$$C = \frac{22.4 \times \rho \times d \times V_1}{V_2 \times M \times 10^{-9}}$$

where $C$ (ppm) denotes the concentration of the gas to be measured, $\rho$ denotes the purity of the liquid, $d$ (g/mL) denotes the density of the liquid, $V_1$ (mL) denotes the volume of the liquid, $V_2$ (mL) denotes the volume of the gas chamber, and $M$ (g/mol) denotes the molecular weight of the gas to be measured.

## 3. Results and Discussion

Figure 1 shows the XRD results of the obtained rodlike GdFeO$_3$ and butterflylike GdFeO$_3$ materials. The samples were well crystallized into an orthorhombic phase, as the diffraction peaks were intensive, narrow, and matched well with the standard card (JCPDS No. 74-1476) with a perovskite structure.
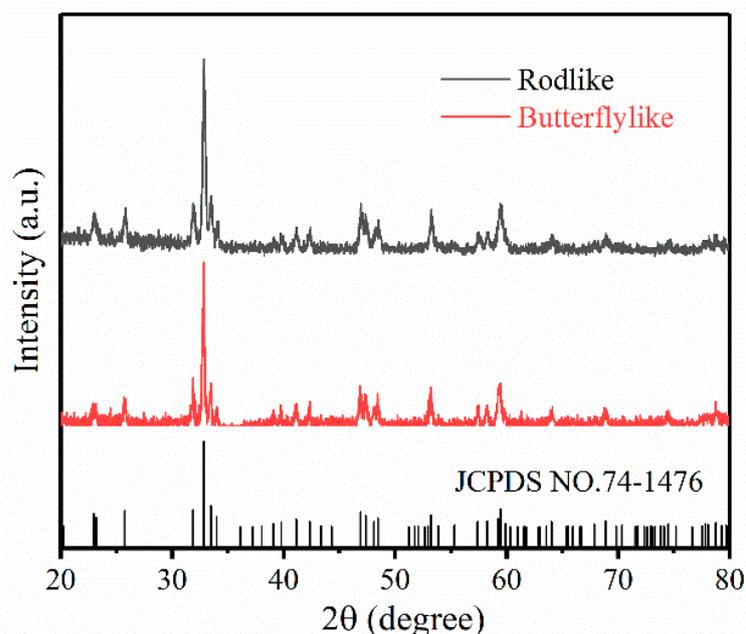


**Figure 1.** XRD results of rodlike GdFeO$_3$ and butterflylike GdFeO$_3$ materials.

Figure 2 shows the SEM images of GdFe(CN)$_6$·4H$_2$O precursors and GdFeO$_3$ with the morphologies of rod and butterfly. The precursor with a rod structure had a diameter of 109.3 nm and a length of 1.536 μm, with smooth surface characteristics (Figure 2a). After calcination, the GdFe(CN)$_6$·4H$_2$O rods changed into GdFeO$_3$. Figure 2b shows that the GdFeO$_3$ was still a rod-shaped structure. Its diameter and length underwent no significant change compared with the precursor. However, the surface of GdFeO$_3$ was rougher, due to the gaps and cavities between GdFeO$_3$ nanoparticles caused by the annealing process. This form of GdFeO$_3$ can provide abundant active sites, enhance gas-adsorption capacity, and improve the gas-sensing performance of the material. Figure 2c presents the butterflylike GdFe(CN)$_6$·4H$_2$O precursor, with a length of about 6.208 μm and a thickness of 359.9 nm. The butterflies have a multi-level structure, so the surfaces around them are not very smooth. The GdFeO$_3$ synthesized from the butterfly-shaped precursor was the shape and size as the precursor. However, the surface of the particles became rougher (Figure 2d). The GdFeO$_3$ butterfly did not exhibit obvious porosity, which is unfavorable for gas-sensing performance.

For detecting gas-sensing performances of the synthesized GdFeO$_3$ rods and GdFeO$_3$ butterflies, the materials were made into gas-sensing devices. The responses of the devices are defined as $R_g/R_a$, as the GdFeO$_3$ rods and GdFeO$_3$ butterflies are p-type semiconductors, and their resistances increase when they encounter reducing gases.
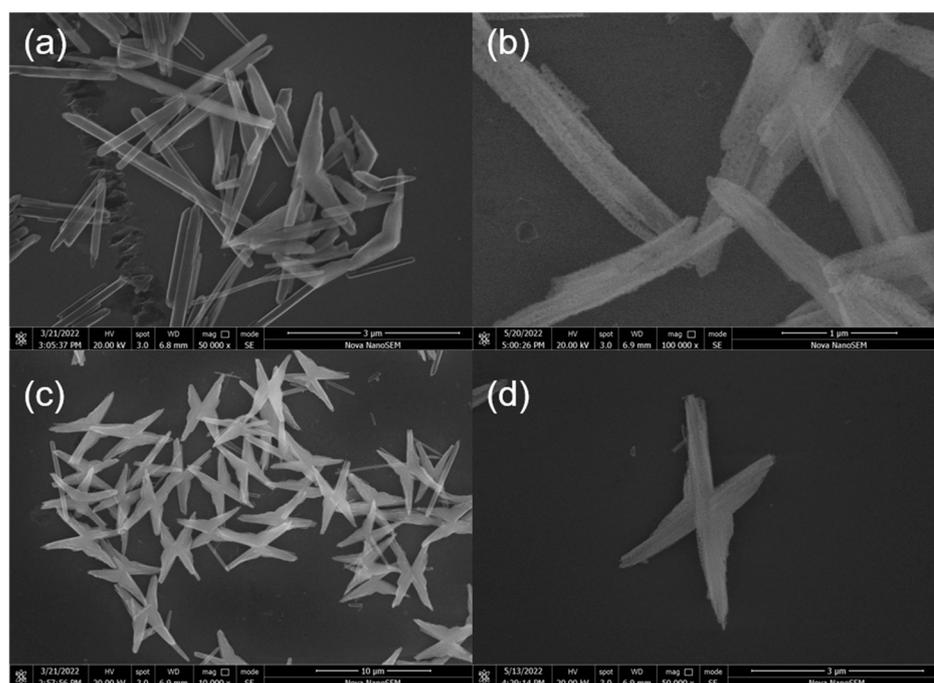
**Figure 2.** SEM images of GdFe(CN)$_6$·4H$_2$O rods precursors (**a**), butterflies (**c**) precursors; SEM images of GdFeO$_3$ rods (**b**) and butterflies (**d**).

It is known that the corresponding response value of the gas sensor usually depends on the working temperature, because the temperature has a great impact on the reaction kinetics of the gas on the surface of the sensing material. At the same time, the working temperature also has a direct impact on the safety and energy consumption of the sensor. A higher temperature means higher energy consumption and danger in testing flammable and explosive gases. Therefore, in order to determine the optimal operating temperature of the sensor, the responses to five different reducing gases with a concentration of 100 ppm were measured at a temperature range of 100–200 °C. For the sensor based on the GdFeO$_3$ rods, it can be seen from Figure 3a that the responses to all the target gases with the same concentration present a curve form of "rise–peak–fall" in response to temperature. The explanation of this phenomenon is as follows: when the sensor is at a relatively low temperature, the target gas molecule does not have enough thermal energy to overcome the activation energy barrier, so that it cannot fully react with a small amount of O$^-$ and O$_2{}^-$ adsorbed on the material surface, resulting in a low corresponding value of the gas sensor. With the increase of working temperature, not only do the target gas molecules have more energy to overcome the activation energy barrier, but there are also more reactive oxygen species on the surface of gas-sensing materials. These two factors lead to the increase in the response value of the sensor. When the operating temperature of the sensor is higher than the optimal operating temperature, the gas molecules adsorbed escape before reacting, thus the response value of the sensor may be reduced [26,27]. The sensor based on GdFeO$_3$ rods had no response value when the temperature is lower than 100 °C, and reached its maximum at 140 °C towards 100 ppm acetone (C$_3$H$_6$O), n-propanol (C$_3$H$_7$OH), isopropanol (C$_3$H$_8$O), methanol (CH$_3$OH), and ethanol (C$_2$H$_5$OH), respectively. Therefore, we can determine that 140 °C is the optimal operating temperature of the sensor, and take this temperature as the actual working temperature for the further study of gas-sensing performance. For the sensor based on the GdFeO$_3$ butterflies, it can be seen from Figure 3b that the responses to all target gases show curves form of "decrease" with respect to temperature. The explanation of this phenomenon is as follows: the optimal operating temperature of the gas-sensing material is likely to be lower than 120 °C, but the performance cannot be detected at temperatures below 120 °C as the resistance of the sensor exceeds the range of the instrument. Therefore, the temperature always exceeded

the optimal operating temperature, and the response value of gas sensor always decreased with the increase of temperature. The response values of the gas sensor based on GdFeO$_3$ butterflies to acetone, n-propanol, isopropanol, methanol, and ethanol with a concentration of 100 ppm reached the maximum at 120 °C. The working temperatures of the two sensors are relatively low, which can reduce energy consumption and ensure the safety of the gas sensor when it is used for detecting flammable and explosive gas. Although the optimal working temperature of the sensor based on GdFeO$_3$ rods is a little higher than that of GdFeO$_3$ butterflies, the largest response of the sensor based on GdFeO$_3$ rods (58.113 to 100 ppm n-propanol) was about three times larger than that of GdFeO$_3$ butterflies (19.515 to 100 ppm n-propanol). The higher response of the GdFeO$_3$ rods-based sensor than the GdFeO$_3$ butterflies can be attributed to the porous structure of the GdFeO$_3$ rods.
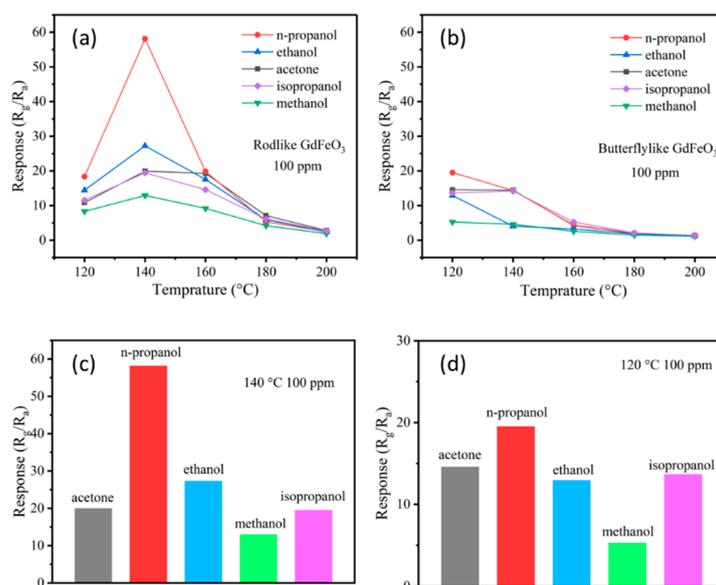


**Figure 3.** The relationship between temperature and response to 100 ppm different gases of the sensors based on GdFeO$_3$ rods (**a**) and GdFeO$_3$ butterflies (**b**). The selectivity of the sensors based on GdFeO$_3$ rods (**c**) and GdFeO$_3$ butterflies (**d**).

The selectivity of a sensor is also considered to be one of the important factors in its practical application. When the sensor is exposed to an environment containing a variety of gases, it is necessary to detect specific gas accurately. Under the same circumstances, the responses of the gas sensor based on GdFeO$_3$ rods to acetone, n-propanol, ethanol, methanol, and isopropanol with a concentration of 100 ppm at 140 °C were 19.912, 58.113, 27.227, 12.922, and 19.440, respectively, which can be clearly seen from Figure 3c. The gas sensor based on GdFeO$_3$ rods showed the highest sensitivity to n-propanol, more than twice than the responses to the other four gases, indicating that the sensor is a better candidate for detecting n-propanol. However, the selectivity of the sensor based on GdFeO$_3$ butterflies was not so good as that of the sensor based on GdFeO$_3$ rods. The responses to acetone, n-propanol, ethanol, methanol, and isopropanol with a concentration of 100 ppm at 120 °C were 14.552, 19.515, 12.912, 5.26, and 13.663 respectively, which can be clearly seen from Figure 3d. The sensor also exhibited a selectivity to n-propanol gas, but it was not easy to distinguish the responses to n-propanol and the other four gases, except methanol.

Therefore, the rod-like GdFeO$_3$ exhibited much higher responses than the butterfly-like GdFeO$_3$ to all five gases, and better selectivity than the butterfly-like GdFeO$_3$. We mainly discuss the properties of the rod-like GdFeO$_3$ in the following.

The gas sensor based on GdFeO$_3$ rods measured n-propanol gas with a concentration range from 1 to 100 ppm at its optimal operating temperature of 140 °C, and the results are shown in Figure 4a. The results show that the response increased with the increase of gas concentration, with a detection limit of 1 ppm. The linear characteristic is important

in the application of electronic devices. Then, the linear relationship of the response and concentrations from 1 ppm to 100 ppm was fitted, with $R^2$ = 0.99833 (as shown in Figure 4b). The data are well fitted in a line, demonstrating a good ability for quantitative detection of n-propanol.
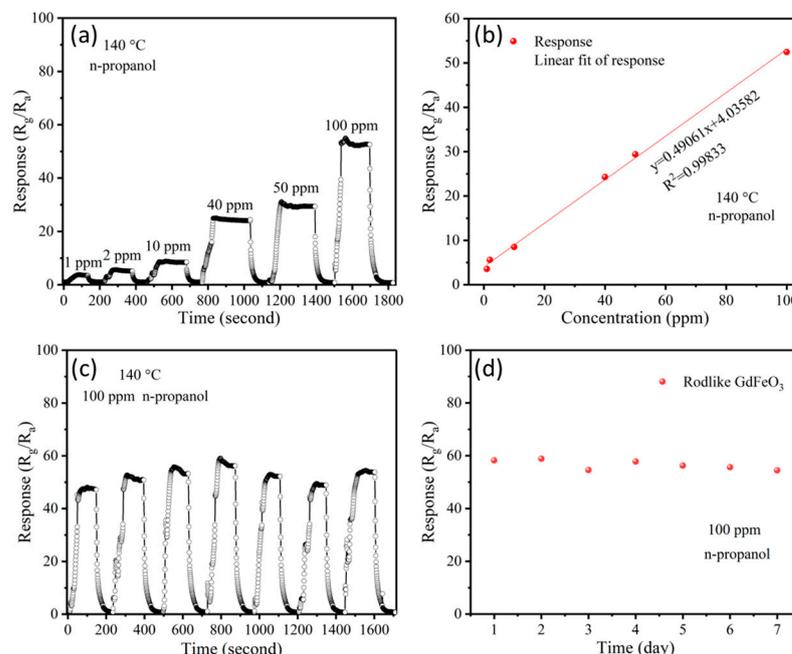


**Figure 4.** (**a**) Dynamic response–recovery transients of sensor based on GdFeO$_3$ rods to increasing concentration of n-propanol from 1 ppm to 100 ppm at 140 °C. (**b**) Linear fitting curves for the response value to n-propanol concentration in the range 1–100 ppm. (**c**) Cycling stability and (**d**) long-term stability of the sensor based on GdFeO$_3$ rods to 100 ppm n-propanol at 140 °C.

In practical application, the stability of a sensor is important for repeated and long-term use. Therefore, the cycling stability was studied by cycling 100 ppm n-propanol and air 5 times at 140 °C (Figure 4c), and the long-term stability of the sensor based on GdFeO$_3$ rods was evaluated for the response to 100 ppm n-propanol at 140 °C for 7 days (Figure 4d). The results show that the sensor based on GdFeO$_3$ rods had almost the same response and recovery characteristics, with roughly equal responses and recovery to the initial status every time, which demonstrated that the sensor based on GdFeO$_3$ rods has good repeatability. In addition, the response varied slightly during the 7 days, indicating good long-term stability of the sensor.

Real-time monitoring requires fast response and recovery. However, for semiconductor material, the working temperature exerts a tremendous influence on the adsorption, desorption, and reaction of gas molecules, in addition to the activity and number of active sites on the material surface. In this study, the operating temperature was 140 °C, which is relatively lower than the conventional rare-earth perovskite oxide semiconductors. The adsorption, desorption, and reaction processes on the material surface will take longer. Response time $\tau_{res}$ and recovery time $\tau_{rec}$ are defined as the time taken by the sensor to reach 90% of the total resistance change under the presence and absence of target gas, respectively. After calculation in Figure 5, the response and recovery time of the gas sensor based on GdFeO$_3$ rods to n-propanol were 28 s and 28 s, respectively. These times are acceptable for actual monitoring.
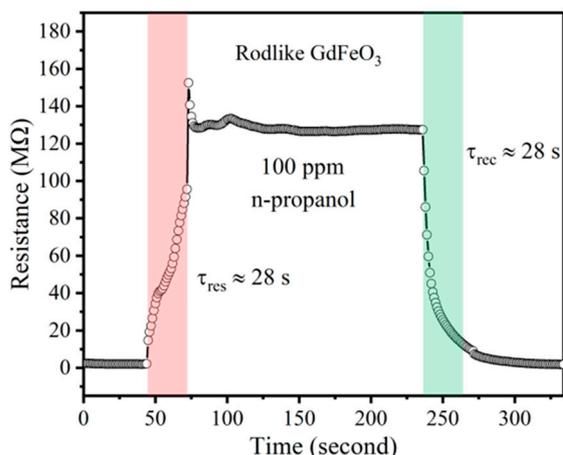
**Figure 5.** The response and recovery times of the sensor based on GdFeO$_3$ rods to 100 ppm n-propanol at 140 °C.

In short, the sensor based on GdFeO$_3$ rods exhibits good gas sensing performance below 100 ppm, which shows that the GdFeO$_3$ rods-based sensor performs well in detecting low-concentration n-propanol.

The gas-sensing mechanism of the sensor based on GdFeO$_3$ is mainly the change of resistance caused by the adsorption and desorption of target gas molecules on the material surface [28,29]. For the GdFeO$_3$ material prepared in this experiment, when the material is in contact with reducing gas, the resistance increases, and when it is in contact with oxidizing gas, the resistance decreases, which is a typical p-type conductive mechanism.

When the GdFeO$_3$ surface is exposed to air, the grain surface adsorbs O$_2$ in the air in the form of physically adsorbed oxygen and chemically adsorbed oxygen. At low temperatures, the adsorbed oxygen on the surface is O$_2^-$. When the temperature increases gradually, the adsorbed oxygen changes to O$^-$, and the formation process is shown in the following reaction formula [30]. Due to the large electronegativity of oxygen, it can capture electrons in GdFeO$_3$ and form an adsorbed oxygen state. Thus, the hole concentration in the valence band increases and the effective carrier concentration increases, thickening the "holes accumulation layer" (as shown in Figure 6), so the resistance decreases.
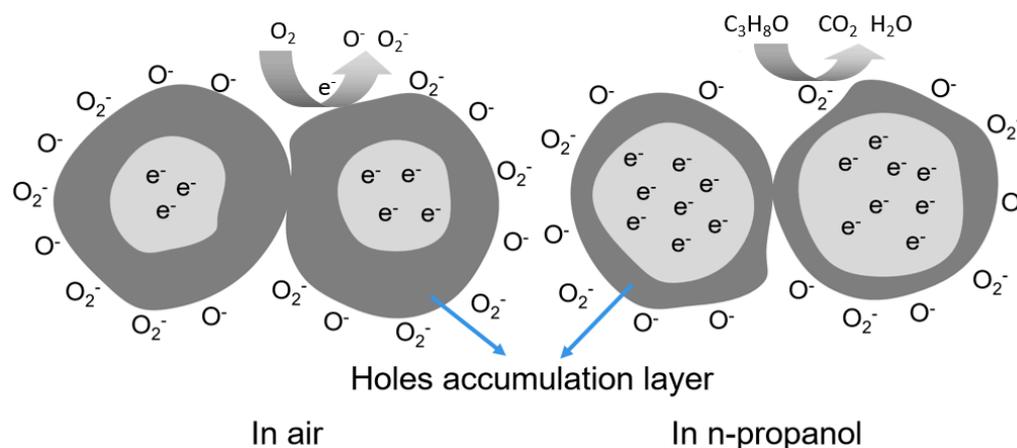


**Figure 6.** A schematic diagram of the n-propanol response mechanism of the sensor based on GdFeO$_3$.

$$O_2 \text{ (gas)} + e^- \rightarrow O_2^- \text{ (ads)} \tag{1}$$

$$O_2 \text{ (gas)} + 2e^- \rightarrow 2O^- \text{ (ads)} \tag{2}$$
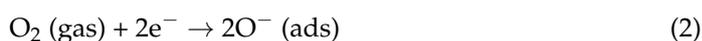
When the reducing gas n-propanol is in contact with the surface of $GdFeO_3$ material, it is not only adsorbed on the surface, but also reacts with the adsorbed oxygen species with high reaction activity:

$$C_3H_8O \text{ (ads)} + 9O^- \text{ (ads)} \rightarrow 3CO_2 + 4H_2O + 9e^- \tag{3}$$

$$2C_3H_8O \text{ (ads)} + 9O_2^- \text{ (ads)} \rightarrow 6CO_2 + 8H_2O + 9e^- \tag{4}$$
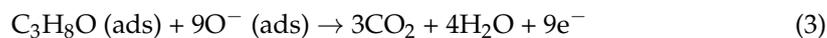
Electrons are released and combined with holes:

$$h' + e' \rightarrow 0 \tag{5}$$

At this time, the "holes accumulation layer" is thinned, the resistance of the material increases, and the conductivity decreases, so as to detect the reducing gas n-propanol.

Comparing the two kinds of $GdFeO_3$, we obtain the following information: from the SEM results, the size of the $GdFeO_3$ rod is much smaller than that of the $GdFeO_3$ butterfly, and the rod is more porous and looser than the butterfly. In other words, there are more active sites of $GdFeO_3$ rod than butterfly. This makes the device have a higher response to the target gas under the same conditions, which corresponds with the results of the gas-sensing test.

Regarding the good gas-sensing performance of $GdFeO_3$ rods, the results of XPS analysis may give a reasonable explanation. XPS was applied to investigate the chemical composition and valence states of elements in the samples. The survey spectrum indicated the elemental composition of Gd 4d, Fe 2p, and O 1s in $GdFeO_3$ in addition to the reference charge correction carbon peak, C 1s, at 284.6 eV (as shown in Figure 7a). Figure 7b shows the high-resolution spectrum of the Gd 4d peak. Gd 4d has three peaks at 141.6 eV, 143.64 eV, and 147.69 eV, representing Gd $4d_{5/2}$ and Gd $4d_{3/2}$ [31]. The high-resolution XPS spectrum of the Fe is shown in Figure 7c. The peaks at 710.49 eV and 712.55 eV of the Fe 2p spectrum correspond to $Fe^{3+}$ and $Fe^{4+}$ respectively [8]. For defect-free $GdFeO_3$ crystal, all Fe ions should be $Fe^{3+}$. However, in the real structure, some $Fe^{3+}$ will be transformed into $Fe^{4+}$ to keep the whole material electricity-neutral, due to the anion vacancy as well as adsorbed oxygen species. Furthermore, the oxygen status plays a key role in gas-sensing processes. Figure 7d presents the XPS spectrum of O 1s in $GdFeO_3$ rods and the coherent fitting of three components. The lattice oxygen ($O_L$) component of O 1s spectra centered at ca. 528.78 eV is attributed to the lattice oxygen in the $GdFeO_3$ phase, the defect oxygen ($O_V$) component at ca. 530.84 eV is associated with $O^{2-}$ ions in oxygen-deficient regions of $GdFeO_3$, and the adsorbed oxygen component at ca. 532.62 eV is attributed to chemisorbed and dissociated oxygen species ($O_2^-$, $O^-$ or $O^{2-}$) and $OH^-$ [32]. The percentages of lattice oxygen, defect oxygen, and adsorbed oxygen are calculated to be 47.9%, 37.5%, and 14.6%, respectively. The good gas-sensing performance of $GdFeO_3$ rods may be due to the high content of defect oxygen and adsorbed oxygen [33]. Herein, the adsorbed oxygen species on the surface of $GdFeO_3$ rods reacts with the target gas of reducing molecules, increasing the concentration of hole carriers, thus contributing to the response value of the sensor. In addition, the defect oxygen can act as active sites for molecule adsorption, boosting the gas-sensing performance of the sensor based on $GdFeO_3$ rods [34].
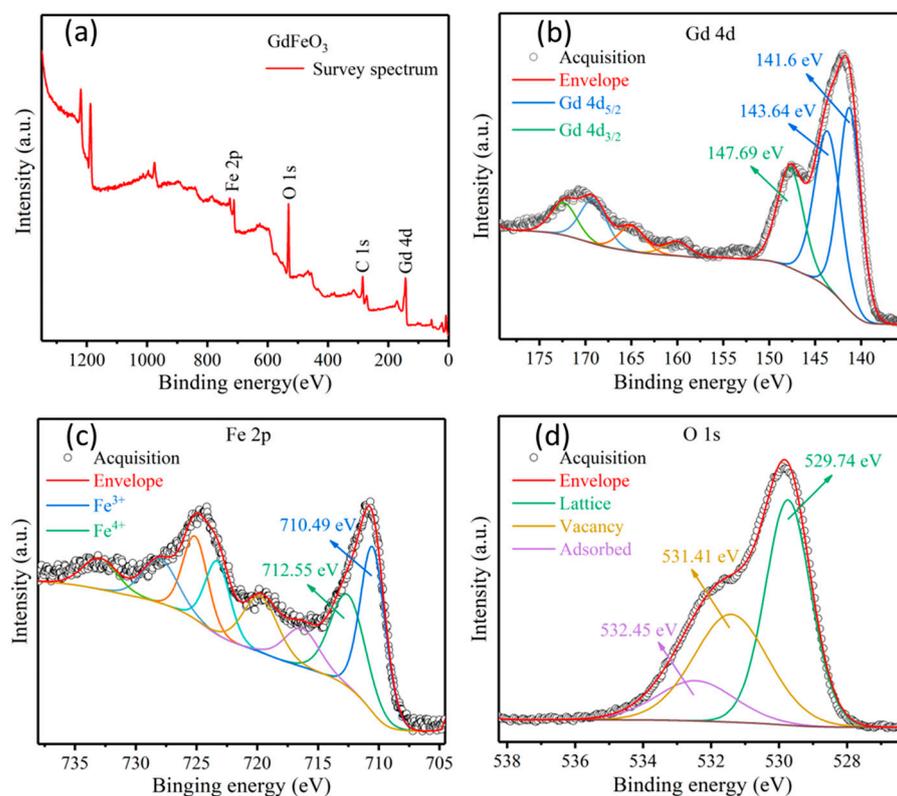
**Figure 7.** XPS survey (**a**) and high-resolution scan of Gd (**b**), Fe (**c**) and O (**d**) elements of GdFeO$_3$ rods.

## 4. Conclusions

In summary, precursors of GdFe(CN)$_6$·4H$_2$O rods and butterflies were synthesized by a convenient and eco-friendly co-precipitation methodology via morphological regulation and control. After annealing at 800 °C for 3 h, the GdFeO$_3$ rods and butterflies were obtained. Characterization of GdFeO$_3$ and GdFe(CN)$_6$·4H$_2$O was confirmed through XRD, SEM, and XPS. Gas-sensing tests showed that the optimum operating temperatures of sensors based on GdFeO$_3$ rods and butterflies are 140 °C and 120 °C, respectively. Each of the sensors based on the two materials exhibited higher response to n-propanol than to other four gases, and the sensor based on GdFeO$_3$ rods possessed better selectivity. The sensor based on GdFeO$_3$ rods also showed a good linear relationship between the response and the concentration of n-propanol from 1 ppm to 100 ppm. In addition, it also has good repeatability and short response/recovery time. Therefore, GdFeO$_3$ rods may play an important role in the actual application of n-propanol detection. The strategy of material synthesis and morphology control provides an approach to prepare high-performance gas-sensing materials.

**Author Contributions:** Conceptualization, X.W.; methodology, J.L. and G.Z.; investigation, J.L., N.L., T.Z. and G.Z.; resources, X.W.; data curation, N.L., T.Z., H.L. and G.Z.; writing—original draft preparation, J.L., T.Z. and X.W.; writing—review and editing, J.L., N.L., H.L., G.Z. and X.W.; visualization, J.L., N.L., H.L. and T.Z.; supervision, X.W.; project administration, X.W.; funding acquisition, J.L. All authors have read and agreed to the published version of the manuscript.

**Conflicts of Interest:** The authors declare no conflict of interest.

## References

1. Arafat, M.M.; Dinan, B.; Akbar, S.A.; Haseeb, A. Gas Sensors Based on One Dimensional Nanostructured Metal-Oxides: A Review. *Sensors* **2012**, *12*, 7207–7258. [CrossRef]
2. Yang, S.X.; Jiang, C.B.; Wei, S.H. Gas sensing in 2D materials. *Appl. Phys. Rev.* **2017**, *4*, 021304. [CrossRef]

3. Comini, E.; Faglia, G.; Sberveglieri, G.; Pan, Z.W.; Wang, Z.L. Stable and highly sensitive gas sensors based on semiconducting oxide nanobelts. *Appl. Phys. Lett.* **2002**, *81*, 1869–1871. [CrossRef]

4. Bulemo, P.M.; Kim, I.D. Recent advances in $ABO_3$ perovskites: Their gas-sensing performance as resistive-type gas sensors. *J. Korean Ceram. Soc.* **2020**, *57*, 24–39. [CrossRef]

5. Hao, P.; Qiu, G.; Song, P.; Yang, Z.X.; Wang, Q. Construction of porous $LaFeO_3$ microspheres decorated with NiO nanosheets for high response ethanol gas sensors. *Appl. Surf. Sci.* **2020**, *515*, 146025. [CrossRef]

6. Zhang, G.; Song, X.-Z.; Wang, X.-F.; Liu, N.; Li, X.; Wei, Z.; Qian, G.; Wang, Z.; Yu, S.; Tan, Z. $LnFeO_3$ (Ln=La, Nd, Sm) derived from bimetallic organic frameworks for gas sensor. *J. Alloys Compd.* **2022**, *902*, 163803. [CrossRef]

7. Wang, X.F.; Li, X.; Zhang, G.Z.; Liu, N.N.; Liang, H.J.; Wang, Z.H.; Tan, Z.Q.; Song, X.Z. $La[Fe(CN)_6] \cdot 5H_2O$-derived $LaFeO_3$ hexagonal nano-sheets as low-power n-propanol sensors. *Appl. Phys. A* **2022**, *128*, 829. [CrossRef]

8. Gu, J.; Zhang, B.; Li, Y.; Xu, X.; Sun, G.; Cao, J.; Wang, Y. Synthesis of spindle-like Co-doped $LaFeO_3$ porous microstructure for high performance n-butanol sensor. *Sens. Actuators B Chem.* **2021**, *343*, 130125. [CrossRef]

9. Yang, K.; Ma, J.; Qiao, X.; Cui, Y.; Jia, L.; Wang, H. Hierarchical porous $LaFeO_3$ nanostructure for efficient trace detection of formaldehyde. *Sens. Actuators B Chem.* **2020**, *313*, 128022. [CrossRef]

10. Chumakova, V.; Marikutsa, A.; Platonov, V.; Khmelevsky, N.; Rumyantseva, M. Distinct Roles of Additives in the Improved Sensitivity to CO of Ag- and Pd-Modified Nanosized $LaFeO_3$. *Chemosensors* **2023**, *11*, 60. [CrossRef]

11. Sheng, H.; Ma, S.Y.; Han, T.; Yun, P.D.; Yang, T.T.; Ren, J.F. A highly sensitivity and anti-humidity gas sensor for ethanol detection with $NdFeO_3$ nano-coral granules. *Vacuum* **2022**, *195*, 110642. [CrossRef]

12. Huang, H.T.; Zhang, W.L.; Zhang, X.D.; Guo, X. $NO_2$ sensing properties of $SmFeO_3$ porous hollow microspheres. *Sens. Actuators B Chem.* **2018**, *265*, 443–451. [CrossRef]

13. Zhang, Y.; Zheng, A.; Yang, X.; He, H.; Fan, Y.; Yao, C. Cubic $GdFeO_3$ particle by a simple hydrothermal synthesis route and its photoluminescence and magnetic properties. *CrytEngComm* **2012**, *14*, 8432. [CrossRef]

14. Prakash, B.J.; Rudramadevi, B.H.; Buddhudu, S. Analysis of Ferroelectric, Dielectric and Magnetic Properties of $GdFeO_3$ Nanoparticles. *Ferroelectr. Lett.* **2014**, *41*, 110–122. [CrossRef]

15. Yu, H.; Deng, Y.; Chen, B.; Zhang, Y.; Zhao, H. Electrospinning Preparation and Electrochemical Properties of $BiFeO_3$ and $GdFeO_3$ Nanofibers for their Potential Lithium-Ion Battery Applications. *J. Electron. Mater.* **2023**, *52*, 3008–3017. [CrossRef]

16. Li, L.; Wang, X.; Lan, Y.; Gu, W.; Zhang, S.L. Synthesis, Photocatalytic and Electrocatalytic Activities of Wormlike $GdFeO_3$ Nanoparticles by a Glycol-Assisted Sol-Gel Process. *Ind. Eng. Chem. Res.* **2013**, *52*, 9130–9136. [CrossRef]

17. Wang, X.; Ma, W.; Sun, K.; Hu, J.; Qin, H. Nanocrystalline $Gd_{1-x}Ca_xFeO_3$ sensors for detection of methanol gas. *J. Rare Earth.* **2017**, *35*, 690–696.

18. Lee, K.; Hajra, S.; Sahu, M.; Mishra, Y.K.; Kim, H.J. $Co^{+3}$ substituted gadolinium nano-orthoferrites for environmental monitoring: Synthesis, device fabrication, and detailed gas sensing performance. *J. Ind. Eng. Chem.* **2022**, *106*, 512–519. [CrossRef]

19. Balamurugan, C.; Song, S.J.; Lee, D.W. Porous nanostructured $GdFeO_3$ perovskite oxides and their gas response performance to $NO_x$. *Sens. Actuators B Chem.* **2018**, *272*, 400–414. [CrossRef]

20. Wang, X.-F.; Liu, N.; Liang, H.; Wu, H.; Wan, Z.; Meng, Y.; Tan, Z.; Song, X.-Z. Ultrafast synthesized $LaFeO_3$-based oxides for highly sensitive n-propanol sensor. *J. Alloys Compd.* **2023**, *954*, 170217. [CrossRef]

21. Qu, F.; Jiang, H.; Yang, M. Designed formation through a metal organic framework route of $ZnO/ZnCo_2O_4$ hollow core-shell nanocages with enhanced gas sensing properties. *Nanoscale* **2016**, *8*, 16349–16356. [CrossRef] [PubMed]

22. Koo, W.T.; Yu, S.; Choi, S.J.; Jang, J.S.; Cheong, J.Y.; Kim, I.D. Nanoscale PdO Catalyst Functionalized $Co_3O_4$ Hollow Nanocages Using MOF Templates for Selective Detection of Acetone Molecules in Exhaled Breath. *ACS Appl. Mater. Interfaces* **2017**, *9*, 8201–8210. [CrossRef]

23. Wang, X.-F.; Ma, W.; Jiang, F.; Cao, E.-S.; Sun, K.-M.; Cheng, L.; Song, X.-Z. Prussian Blue analogue derived porous $NiFe_2O_4$ nanocubes for low-concentration acetone sensing at low working temperature. *Chem. Eng. J.* **2018**, *338*, 504–512. [CrossRef]

24. Li, P.; Ren, J.; Li, C.; Li, J.; Zhang, K.; Wu, T.; Li, B.; Wang, L. MOF-derived defect-rich $CeO_2$ as ion-selective smart artificial SEI for dendrite-free Zn-ion battery. *Chem. Eng. J.* **2023**, *451*, 138769. [CrossRef]

25. Hussain, I.; Sahoo, S.; Hussain, T.; Ahmad, M.; Javed, M.S.; Lamiel, C.; Gu, S.; Kaewmaraya, T.; Sayed, M.S.; Zhang, K. Theoretical and Experimental Investigation of In Situ Grown MOF-Derived Oriented Zr-Mn-oxide and Solution-Free CuO as Hybrid Electrode for Supercapacitors. *Adv. Funct. Mater.* **2022**, *33*, 2210002. [CrossRef]

26. Neri, G.; Bonavita, A.; Micali, G.; Rizzo, G.; Callone, E.; Carturan, G. Resistive CO gas sensors based on $In_2O_3$ and $InSnO_x$ nanopowders synthesized via starch-aided sol-gel process for automotive applications. *Sens. Actuators B Chem.* **2008**, *132*, 224–233. [CrossRef]

27. Zhou, X.; Liu, J.Y.; Wang, C.; Sun, P.; Hu, X.L.; Li, X.W.; Shimanoe, K.; Yamazoe, N.; Lu, G.Y. Highly sensitive acetone gas sensor based on porous $ZnFe_2O_4$ nanospheres. *Sens. Actuators B Chem.* **2015**, *206*, 577–583. [CrossRef]

28. Yamazoe, N.; Shimanoe, K. Theory of power laws for semiconductor gas sensors. *Sens. Actuators B Chem.* **2008**, *128*, 566–573. [CrossRef]

29. Dey, A. Semiconductor metal oxide gas sensors: A review. *Mater. Sci. Eng. B* **2018**, *229*, 206–217. [CrossRef]

30. Qin, W.B.; Zhang, R.Z.; Yuan, Z.Y.; Shen, Y.B.; Wang, G.M.; Meng, F.L. Exposure Surface Active Sites of Perovskite-Type $LaFeO_3$ Gas Sensors by Selectively Dissolving La Cations for Enhancing Gas Sensing Properties to Acetone. *Adv. Mater. Technol.* **2022**, *7*, 2200255. [CrossRef]

31. Ujwal, M.P.; Yashas, S.R.; Shivaraju, H.P.; Kumara Swamy, N. Gadolinium ortho-ferrite interfaced polyaniline: Bi-functional catalyst for electrochemical detection and photocatalytic degradation of acetaminophen. *Surf. Interfaces* **2022**, *30*, 101878. [CrossRef]

32. Lu, Y.; Zhan, W.; He, Y.; Wang, Y.; Kong, X.; Kuang, Q.; Xie, Z.; Zheng, L. MOF-templated synthesis of porous $Co_3O_4$ concave nanocubes with high specific surface area and their gas sensing properties. *ACS Appl. Mater. Interfaces* **2014**, *6*, 4186–4195. [CrossRef] [PubMed]

33. Liu, H.; Zhu, D.; Miao, T.; Liu, W.; Chen, J.; Cheng, B.; Qin, H.; Hu, J. Highly Sensitive p-$SmFeO_3$/p-$YFeO_3$ Planar-Electrode Sensor for Detection of Volatile Organic Compounds. *Chemosensors* **2023**, *11*, 187. [CrossRef]

34. Tong, B.; Deng, Z.; Xu, B.; Meng, G.; Shao, J.; Liu, H.; Dai, T.; Shan, X.; Dong, W.; Wang, S.; et al. Oxygen Vacancy Defects Boosted High Performance p-Type Delafossite $CuCrO_2$ Gas Sensors. *ACS Appl. Mater. Interfaces* **2018**, *10*, 34727–34734. [CrossRef] [PubMed]